Journal of Institute of Science and Technology, 31(1), 183-202 (2026)
ISSN: 2467-9062 (print), e-ISSN: 2467-9240
https://doi.org/ 10.3126/jist.v31i1.92864

Research Article

INVESTIGATION ON ANTI-CORROSIVE CONSEQUENCES OF *LITSEA MONOPETALA* (ROXB) PERS LEAF EXTRACT ON MILD STEEL IN SIMULATED INDUSTRIALLY POLLUTED CONCRETE ELECTROLYTE

Nootan Prasad Bhattarai[1], Utshav Pokharel[1], Rajanraj Thapa[1], Kamal Thapa Kunwar Magar[1], Yuvraj Paudel[1], Dhruba Babu Subedi[1], Jagadeesh Bhattarai[1*]

[1]*Central Department of Chemistry, Tribhuvan University, Kirtipur 44618, Kathmandu, Nepal*
**Correspondence: bhattarai_05@yahoo.com; jagadeesh.bhattarai@cdc.tu.edu.np*

(*Received*: April 13, 2026; *Final Revision*: May 20, 2026; *Accepted*: June 8, 2026)

ABSTRACT

Outstanding compressive and tensile forces make reinforced concrete systems versatile and popular in construction and technology engineering. Preliminary corrosion damage of reinforcing mild steel (MS) in sulfate-polluted environments in industrial (IndE) areas is becoming a significant problem. This investigation examines for the first time the anti-corrosion efficiency and mechanisms of reinforced MS rebars in simulated concrete pore solution (SCPS, a mimic of the concrete matrix) with 500-2000 ppm leaf extract of *Litsea monopetala* (Roxb) Pers (LmL), which has a pH of around 12.5±0.5, providing insight into concrete corrosion preventive strategies. To assess the anti-corrosion efficiency and mechanisms of LmL on mild steel (MS) rebars, potentiodynamic polarization (PDP), cyclic voltammetry (CV), electrochemical impedance spectrometry (EIS), and adsorption isotherm methods were utilized at 30 °C. This evaluation included LmL characterization techniques such as screening tests, UV-Vis spectrometry, FTIR, GC-MS spectrometry, and toxicity analysis. The results showed an anti-corrosion efficiency of 79.77% based on corrosion current ($IE_{icorros}$) from Tafel plots, and 62.82% based on the I_{peak} from CV (IE_{Ipeak}), and 97.63% based on the EIS method (IE_{Rct}) at a concentration of 2000 ppm of LmL in SCPS under IndE (SCPS-IndE) at 30 °C. These findings suggest that 500-2000 ppm MaL significantly improved the corrosion-resistant behavior of MS in simulated concrete systems under sulfate-polluted industrial environments. The secondary metabolites in LmL, primarily flavonoids, alkaloids, and carboxylic and phenolic acids, inhibit both anodic and cathodic reactions, which enhances anti-corrosion properties by forming a passive layer on corroded MS surfaces.

Keywords: Concrete pore system, Corrosion-resistant efficacy, EIS, *Litsea monopetala* extract, Mixed inhibitor

INTRODUCTION

Concrete structures largely dominate urban areas in Nepal due to rapid urbanization and the necessity for buildings that are stable, durable, and resistant to seismic activity. Nowadays, concrete has become one of the preferred construction materials in Nepal due to its high compressive strength, which ranges from 15 MPa to over 40 MPa, as documented elsewhere (Jagadesh et al., 2021). The tensile strength of the concrete structure is 10% of the compressive strength (Iskhakov & Ribakov, 2021). Consequently, it is assumed that low tensile strength, ranging from 2-5 MPa, is compared to the compressive strength. The tensile strength of concrete is enhanced by reinforcing it with mild steel or metal rebars to effectively manage structural loads in reinforced concrete infrastructures (ReCIs). The durability of the reinforcing MS in concrete infrastructures is also attributable to the high alkalinity nature of the concrete pore solution with a pH range of 12.5-13.5 (Jabed et al., 2023).

However, the negative effects on the stability and durability are posed by environmental pollutants (such as chlorides and sulfate ions, SO_2 and carbon dioxide gases, including moisture content), which can weaken the structural integrity of the ReCIs (Thakur et al., 2025). It may lower the pH to 10 or below within the concrete environments (Bhattarai, 2010). Then the corrosive degradation of the reinforcing steel leads to the formation of voluminous rust products, which enhances the development of internal force (Thapa Kunwar Magar et al., 2025). This force eventually exceeds the concrete's tensile strength, resulting in cracking, delamination, and spalling, which further accelerates corrosive degradation by creating pathways for aggressive species to reach the surface of the MS embedded in the concrete matrix or the concrete pore solution, particularly in the harsh

industrial and marine environments (Keles et al., 2023). One of the intrinsic limitations of ReCIs in urban areas is the premature corrosion of reinforcing metals within the concrete or concrete pore solution (Phulara & Bhattarai, 2019). Early corrosion of the reinforcing steel is a noteworthy concern across various industrial and technological sectors, including construction (Arya et al., 2020), hydropower and dam projects (Jianxia, 2012), concrete bridges (Wilkie & Dyer, 2021), flyovers, and tunnel construction (Li et al., 2019).

Such corrosion issues in reinforced concrete are solved using various techniques and chemicals. In recent decades, the use of plant-based phyto-chemicals (PBPCs) derived from the waste parts of the plant bodies has emerged as the most effective eco-friendly method for reducing the corrosive degradation of metal infrastructures in various electrolytes, such as the leaf extracts of *Catharanthus roseus* in 0.5 M NaCl (Rana et al., 2017), *Vitex negundo* in biodisel and bleded (Subedi et al., 2019), *Aegle marmelos* and *Elaeocarpus ganitrus* in bio-ethanol (Katuwal et al., 2020), Flossflower and Yam in reinforced concrete (Pandey et al., 2024), *Ziziphus budhensis* and *Tagetes erecta* in concrete (Gautam et al., 2024), and *Sesamum indicum* in concrete pore solution (Gautam et al., 2025a); stem extracts of *Ziziphus joazeiro* in acid (Mauro et al., 2021) and *Tinospora cordifolia* in biodiesel-based fuels (Amgain et al., 2022), and bark extracts of white turnip in acid (Alemnezhad et al., 2023) and *Phyllanthus emblica* in reinforced concrete (Gautam et al., 2025b) are widely exploited as anti-corrosive chemicals to reduce the early degradation of metals in corrosive electrolytes.

These PBPCs demonstrated anti-corrosion efficiencies ranging from 80% to 95%, comparable to conventional inhibitors (nitrites, nitrates, molybdates, chromates, polyphosphates, waterproofing chemicals, amines, and others). On the other side, the PBPCs have superior anti-corrosive properties compared to conventional synthetic inorganic and organic chemicals (Rutsa et al., 2026). The conventional synthetic inorganic and organic chemicals are more toxic and pose environmental hazards (Alvarez et al., 2023). Even the synthetic waterproofing chemicals used as concrete additives are not environmentally friendly and showed less effective anti-corrosion behavior after 3 months, as reported in the literature (Roka et al., 2023). Many waste parts of plants remain unexplored in the formulation of concrete additives with anti-corrosive efficiency aspects. This study aims to substitute synthetic inorganic and organic corrosion inhibitors with eco-friendly, cost-effective alternatives derived from methanol extracts of *Litsea monopetala* (Roxb) Pers. leaves.

L. monopetala (Roxb) Pers., a Lauraceae Family and *Litsea* genus plant, known as Kutmiro in Nepali and Common Grey Mango Laurel in English, is distributed in tropical and subtropical areas (up to about 1500 meters altitude) of Nepal (Khanal & Bhatt, 2020). It retains its green leaves throughout the year, which are broadly oval or obovate to ovate-oblong in shape, mostly used for fodder purposes to feed cattle. Phytochemical screening of the methanolic and ethanolic extract of its leaves documented the presence of alkaloids, flavonoids, polyphenols, glycosides, terpenoids, steroids, saponins, and carbohydrates in the literature (Arifuzzaman et al., 2025; Labu et al., 2026). The pharmacological potential of *L. monopetala* (Roxb) Pers. leaf extracts was evaluated by analyzing their total bioactive compounds, which demonstrate high antioxidant properties (Hossain et al., 2017).

These bioactive secondary metabolites or phytochemicals contain heteroatoms (oxygen, nitrogen), π-bonds, aromatic ring and conjugated compounds, which are necessary for forming a protective film on metal surfaces, as reported previously (Holla et al., 2024). In addition, these phytochemicals, derived from the methanol leaf extract, exhibited high antioxidant and metal-chelating activity, suggesting a potential for mitigating electrochemical oxidation on metal surfaces that allows us to study the corrosion-inhibiting activities in an aggressive simulated concrete pore solution at an industrially polluted site with an excess number of sulfates.

Phytochemical studies of the leaf extract of the *L. monopetala* (Roxb) Pers strongly indicates its potential as an eco-friendly corrosion inhibitor, even in simulated sulfate-polluted concrete pore solutions that mimic concrete systems. The current efforts focus on developing new, effective anti-corrosive additives derived from Kutmiro (*L. monopetala*) leaves. These additives are intended for use as anti-corrosive additives in a simulated cement pore solution in an industrial environment (SCPS-IndE) with a pH of 12.5 or more, which closely mimics concrete systems exposed to sulfate pollution (Harb et al., 2020).

Under these circumstances, this investigation aims to examine the phytochemicals derived from the leaf powder of *L. monopetala* (Roxb) Pers. (LmL) using ultraviolet-visible (UV-Vis) spectroscopy, Fourier transform infrared (FTIR) spectroscopy, and gas chromatography-mass spectrometry (GC-MS), along with phytochemical screening tests. In addition to

these methods, we analyze the anti-corrosion potential of LmL on mild steel specimens through polarization methods (PDP, CV, and EIS) and various adsorption isotherms (Langmuir, Freundlich, Temkin, and El-Awady). This study provides practical insights for creating sustainable, eco-friendly concrete additives using the methanol leaf extract of *L. monopetala* (Roxb) Pers.

MATERIALS AND METHODS

Preparation of plant extract

Approximately five kilograms of undamaged mature leaves and fruit from a *L. monopetala* tree were collected in Bhadrapur Municipality, Jhapa District, Nepal, located at 26.5444° N and 88.0944° E at 100 m above sea level, as shown in Figure 1. The plant was authenticated as *L. monopetala* (Roxb) Pers. by botanist Dr. Tirtha Raj Pandey, at the National Herbarium and Plant Laboratory in Godavari, Lalitpur, Nepal, with voucher Nos. KATH173341 and KATH173342, and the herbarium specimen was deposited at the same office for future reference.

The fresh and green leaves, as illustrated in Figure 2a, were kept in a shaded area for about thirty days or more to completely dry after removing the unwanted dust attached to the leaf surface by running distilled water over them. The dried leaves were crushed thoroughly using an electric grinder for further processing of the powder preparation method. The leaf powder (400 g) was macerated in 1000 mL of methanol solution (1:2.5 ratio) in a 5000 mL volumetric flask for three weeks or more, with frequent stirring, as shown in Figure 2b. Then, the supernatant of the mixture was filtered. Then, the filtrate, as depicted in Figure 2c containing the phytochemicals, was evaporated using a rotary evaporator of IKA RV 10 digital V model (Germany), as illustrated in Figure 2d, to derive a solid plant extract, abbreviated as LmL, which was stored in the freezer at 4 °C, as in Figure 2e, before use as anti-corrosive phytochemicals, as described elsewhere (Dhungana et al., 2025).

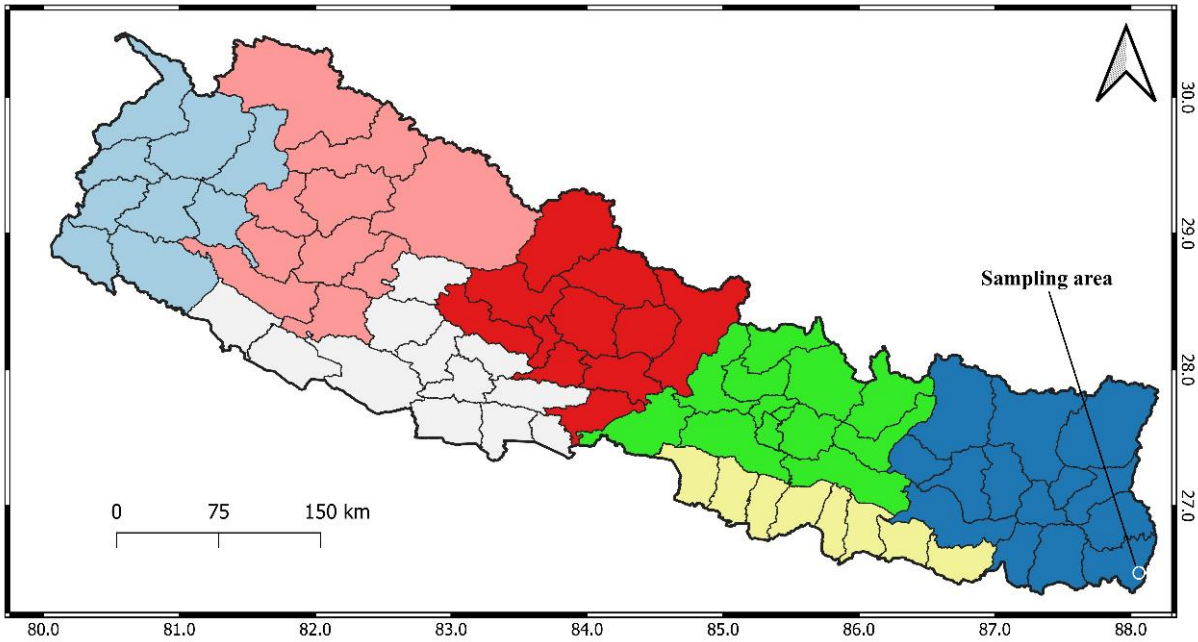

Figure 1. Map of sampling area of leaves of *Litsea monopetala* (Roxb) Pers

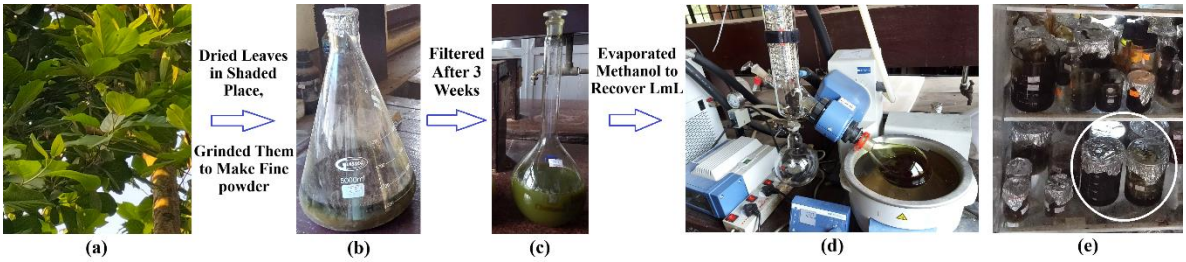

Figure 2. Different steps for the preparation of methanolic extract of *Litsea monopetala* (Roxb) Pers (LmL.)

Analysis techniques for LmL characterization

The electronic transition states, functional groups, type of phytochemicals, and acute oral toxicity (AOT) tests of the LmL extract were investigated using UV-Vis, FTIR, GC-MS analysis, chemical screening, and AOT tests, following established protocols. The UV-Vis spectrum was recorded on a UV-Visible spectrophotometer (SPECORD® 200 PLUS, Germany) in the range of 200 to 800 nm wavelength, revealing distinct peaks that confirm electronic transitions as well as phytochemical classes. Applied an IR Affinity-1S FTIR spectrometer (Shimadzu Corp., Japan) to identify functional groups of secondary phytochemicals in LmL extract. AOT test of the leaf powder and LmL extract was done on female *Albino mice* at the Natural Products Research Laboratory (NPRL), Department of Plant Resources, Thapathali, Kathmandu, a registered Nepal Government Office, following the standard protocol of the OECD TG 425 Up and Down Procedure-2022 (OECD, 2022) with all the laboratory hazard considerations, as described in details elsewhere (Bhattarai et al., 2026).

Preparation of simulated sulfate-contaminated concrete pore solution

To prepare per liter of simulated sulfate-contaminated concrete pore solution, 2 g $CaCO_3$, 0.4 g/L NaOH, 0.56 g/L KOH, and 0.27 g/L $CaSO_4{\cdot}2H_2O$ were dissolved in deionized water, recording a pH of approximately 12.7, which is the simulated concrete pore solution with 0.01 mol NaOH, 0.02 mol KOH, and 0.00157 mol sulfate, abbreviated as SCPS. Furthermore, it added 71 g of anhydrous Na_2SO_4 per liter of the SCPS, which is a model of the industrially contaminated concrete pore solution, and abbreviated as SCPS-IndE hereafter in this document. The addition of 71 g of anhydrous sodium sulfate results in a sulfate concentration of approximately 0.50 mole. Therefore, the SCPS-IndE solution contains approximately 0.50 mol Na_2SO_4, 0.01 mol NaOH, and 0.02 mol KOH. The sparingly soluble salt of $CaCO_3$ (2 g) acts as a buffer to control the pH of the SCPS-IndE solution to a value of around 12.5. To investigate the anti-corrosion efficiency, kinetics, and inhibition mechanism of leaf-based methanol extract of *L. monopetala* (Roxb) Pers., 500-2000 ppm concentrations of *L monopetala* L. leaf extract (LmLE) are added to SCPS-IndE.

Electrochemical analysis by polarization methods

A GAMRY electrochemical working station was used with a three-electrode system at the Department of Chemical Engineering, IIT Guwahati, India, to investigate the electrochemical polarizations. The electrodes consisted of a standard silver-silver chloride electrode (SSCE) as the reference electrode, a platinum mesh as the counter electrode, and a mild steel (MS) plate measuring 2 cm × 2 cm × 0.5 cm as the working electrode. The composition of the mild steel includes 0.17–0.23% carbon (C), 0.70–0.90% manganese (Mn), and 0.035% phosphorus (P), with about 98% iron (Fe) (Gautam et al., 2024).

Arrangement of these three electrodes at equal distances within a Faraday cage contained a blank solution of SCPS-MarE with concentrations of 1000-4000 ppm of MaL. For the electrochemical analysis, the MS sample specimen was initially immersed for 60 minutes to monitor the corrosion potential (CorP). It is the potential at which a steady state is reached in a graph that plots the change in potential against time. Following this, cathodic and anodic polarization (PDP) was performed within a range of ±0.3 V from the CorP, at a scan rate of 1 mV/s. Next, the CV technique was employed with a polarization range of -1.5 V to 1.0 V, using a sweep rate of 0.05 volts/second. EIS was conducted in the frequency range of 100 kHz to 0.01 Hz using an AC voltage of 0.010 V rms and the R(Q(R(QR))) model is used for fitting the obtained EIS data using ZSimpWin 3.20 software. All polarization measurements were repeated three times after immersing the sample for one hour in each fresh solution. Hence, PDP, CV and EIS analysis showed invariant electrochemical effects.

Tafel extrapolation method and anti-corrosion kinetic analysis

A Tafel extrapolation method, used to determine the Tafel parameters, including the current density (i_{corros}), corrosion potential (OCP), Tafel anodic slope (β_{anode}), and Tafel cathodic slope ($\beta_{cathode}$), helps us to understand the anti-corrosion kinetics, mechanisms, and the effectiveness of LmL on mild steel (MS) in a SCPS-IndE. The corrosion rate (in mm/y)-based kinetics was estimated from the estimated i_{corros} in $\mu A/cm^2$ from the linear plots of both the cathodic and anodic PDP curves using equation (1), where equivalent weight of iron (II) (Eq_{wtFe}) = 27.925 g/mole and density of iron (ρ_{Fe}) = 7.87 g/cm^3. Besides, i_{corros} from the Tafel extrapolation plot was used to calculate the anti-corrosion efficiency (IE) of LmL, and kinetics and mechanism of the anti-corrosion enhancement of MS in SCPS-IndE, using equations (2) and (3), respectively.

Tafel extrapolation lines within ±25 mV potential from the OCP were liable to compute the anti-corrosion efficiency (IE) based on the i_{corros} ($IE_{icorros}$) value, following equation (2).

$$\text{Corrosion Rate} = 0.00327 \times i_{corros} \times \frac{Eqwt_{Fe}}{\rho_{Fe}} \quad \ldots (1)$$

$$IE_{icorros}(\%) = \frac{icorros_{control} - icorros_{LmL}}{icorros_{control}} \times 100 \quad \ldots (2)$$

Where, surface coverage (θ) is as in equation (3) below.

$$\theta = \frac{icorros_{control} - icor_{LmL}}{icor_{control}} \quad \ldots (3)$$

Adsorption isotherm model and anti-corrosion mechanism

With the help of the estimated electrochemical properties obtained from equations (1), (2), and (3), we aimed to investigate the adsorption mechanism of LmL-based phytochemicals on the MS surface, in highly reactive sulfate-polluted industrial SCPS environments, using four adsorption isotherm models. From the analysis of these adsorption isotherm models (i.e., Langmuir, Temkin, El-Awady, and Freundlich), thermodynamic properties can be derived from their linear fit plots, as illustrated in equations (4), (5), (6), and (7), respectively. These models describe how the phyto-molecules of LmL replace corrosive molecules or ions from the corroded mild steel surface, resulting in the building of an anti-corrosive and diffusion-barrier passive film between the corroded mild steel surface and the very aggressive environment of SCPS-IndE.

$$\frac{C_{MaL}}{\theta} = \frac{1}{K_{Lan\text{-}ads}} + C_{MaL} \quad \ldots (4)$$

$$\theta = -\frac{2.303}{f}(\log K_{Tem\text{-}ads} + \log C_{MaL}) \quad \ldots (5)$$

$$\log \frac{\theta}{1-\theta} = y \log K_{AEd\text{-}ads} + y \log C_{MaL} \quad \ldots (6)$$

$$\log \theta = \log K_{Fru\text{-}ads} + \frac{1}{n} \log C_{MaL} \quad \ldots (7)$$

Where $K_{Lan\text{-}ads}$, $K_{Tem\text{-}ads}$, $K_{AE\text{-}ads}$, and $K_{F\text{-}ads}$ are the adsorption coefficients of the Langmuir, Temkin, Al-Edway, and Freundlich adsorption plots, respectively; *f* is interaction factor between phyto-molecules, *y* is the number of absorbed molecules occupying on a corroded MS surface, and *n* is the adsorption intensity of the LmL phyto-molecules, as explained elsewhere (Mamudu et al., 2023).

RESULTS AND DISCUSSION

Characterization of plant extract

The LmL extract was characterized in this study using some chemical, chromatographic, and spectrophotometric test methods. The crude methanol extract of *L. monopetala* (Roxb) Pers. (LmL) was subjected to confirmatory qualitative phytochemical screening tests using a standard protocol, as described in detail (Bhattarai et al., 2021). Main phytochemicals were assumed to be the presence of alkaloids, flavonoids, steroids, phenols, resins, glycosides, and saponins, as summarized in Table 1.

These secondary metabolites derived from the LmL extract can act as anti-corrosive compounds to impede MS deterioration in the SCPS-IndE electrolytes, one of the most corrosive industrial pollutants, forming a diffusion barrier and anti-corrosion layers. The phytochemicals ascertained from the screening tests were also consistent with the previously reported results of the leaf extract of *L. monopetala* (Roxb) Pers (Labu et al., 2026), and except the saponin test (Arifuzzaman et al., 2025).

Table 1. Phytochemical constituents in the methanolic leaf extract of *Litsea monopetala*

Assessments	Descriptions	Phytochemicals	Remarks
Lead acetate test	White precipitate observed	Phenolic	Positive
Dragendorff's test	Orange-red precipitate appeared	Alkaloids	Positive
Alkaline reagent test	Strong yellow color developed	Flavonoids	Positive
Salkowski's test	Appeared reddish-brown color	Terpenoids	Positive
Foam test	Formed foam	Saponins	Positive
Liebermann's test	Changed from violet to blue-green	Glycosides	Positive
Ferric chloride test	Deep green color developed	Tannins	Positive
Molisch's test	A ring at interface not formed	Carbohydrates	Negative

The analysis of the GC-MS of the bulk extract of *L. monopetal* leaves (LmL) revealed a variety of phytochemicals (PhytCs), as listed in Table 2. Key SPCs identified include dihydrocaffeic acid (15.90%), N-methyldodecanamide (15.51%), methyl palmitate (14.17%), isophytol (12.52%), methyl stearate (7.94%), methyl tetradecanoate (6.97%), nicotine (6.23%), ethenone (1-(2-hydroxy-6-methoxyphenyl)-3) (3.82%), prenal (3.32%), methyl methanthranilate (3.23%), neophytadiene (3.10%), quercetin/pyrocatechol (1.48%), 3-methylcrotonaldehyde (1.34%), and octadecanoic acid, 2,3-dihydroxypropyl ester (1.02%). In total, 20 peaks were recorded in the GC-MS spectrum on the bulk LmL, representing the PhytCs derived from LmL.

Table 2. Secondary metabolites (PhytCs) supposed to be present in LmL, based on the GC-MS analysis

Peak No.	Ret. Time (Mins.)	Peak Area (%)	Base m/z	Name of LmL-based phytochemicals
1	3.060	3.32	43	Prenal
2	3.167	0.65	44	N,N-Dimethyltryptamine
3	3.500	0.03	43	3-Methylene-7,11-dimethyl-1-dodecene
4	3.869	3.82	151	Ethenone, 1-(2-hydroxy-6-methoxyphenyl)-
5	4.085	6.23	84	Nicotine
6	4.212	6.97	74	Methyl stearate
7	4.330	3.10	68	Neophytadiene
8	4.373	7.94	74	Methyl tetradecanoate
9	4.523	14.17	74	Hexadecanoic acid, methyl ester (methyl palmitate)
10	4.739	15.51	73	N-Methyldodecanamide
11	4.945	15.90	41	Dihydrocaffeic acid
12	5.197	12.52	41	2-Ethyl-1-pyrroline
13	5.390	1.48	65	Quercetin; Pyrocatechol
14	5.523	0.98	74	Eicosanoic acid, methyl ester
15	5.829	0.74	43	Prenal
16	6.843	0.21	74	Hexadecenoic acid, methyl ester
17	7.946	0.83	69	β-Sitosterol; Supraene
18	8.268	1.02	43	Octadecanoic acid, 2,3-dihydroxypropyl ester
19	8.411	1.34	43	3-Methylcrotonaldehyde
20	10.595	3.23	165	Benzoic acid, 2-(methylamino)-, methyl ester

These PhytCs documented in this analysis align with findings from previous studies. Literature reports research on the phytochemical analysis of the bark extract of *L. monopetala*, revealing that the extract is a rich source of flavonoids and phenols, with ten major phytocompounds as listed elsewhere (Sahoo et al., 2024). An investigation on the leaf extract of this plant species identified two types of prenols: tri-*trans* poly-*cis* prenol-15 and its acetylated derivative tri-*trans* poly-*cis* prenol-15 (Kamal et al., 2024). According to LC-QTOF-MS analysis in the literature, these compounds are potential and promising anti-corrosive agents.

In another GC-MS analysis, oxygenated monoterpenes were in the essential oils of 1,8-cineole, linalool, bulnesol, and citral. 1,8-cineole, including decanal and tetradecanal aldehydes in the fruit and the bark oil, respectively, of *L. monopetala* (Mohd Azhar & Wan Aalleh, 2020). The outcome of chemical screening and GC-MS tests indicates that the application of LmL has conceivable anti-corrosive properties, which control premature corrosion damage of MS rebars in industrially polluted concrete systems with high sulfate ions. The predominant molecular structures of the LmL-based PhytCs, displayed in Figure 3, are established on m/z fragmentation values, retention times, and peak areas.

Likewise, UV-visible spectroscopy gives insights into the secondary metabolites found in LmL extract. It detects the presence of conjugated systems, aromatic rings, chromophores, lone pairs of electrons, as well as π and σ bonds. The procedure documents the UV-Vis spectra by counting the absorption of light, which approximates the excitation of electrons from lower-energy molecular orbitals (π or non-bonding orbitals) to higher-energy antibonding orbitals (π*). The LmL extract showed absorption peaks at 206 nm and 275 nm in the UV-Vis spectrum, as shown in Figure 4a, confirming the presence of phenolic and flavonoid compounds in the extract. These results substantiated previous phytochemical investigations and suggest that LmL contains substantial quantities of phenolic and flavonoid compounds with π→π* electronic transition of C=O in aromatic systems (Lai & Sun, 2017), conjugated unsaturated systems (Zgura et al., 2023), and in carbonyl compounds (Fernandes et al., 2019).

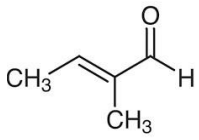

Prenal (**m/z = 43.00**; Rt = 3.060 mins.; terpenoid)

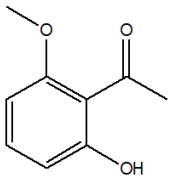

Ethenone, 1-(2-hydroxy-6-methoxyphenyl)- (**m/z = 151**; Rt = 3.869 mins.); phenolic

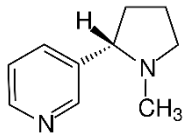

Nicotine (**m/z = 84.00**; Rt = 4.085 mins.; alkaloid)

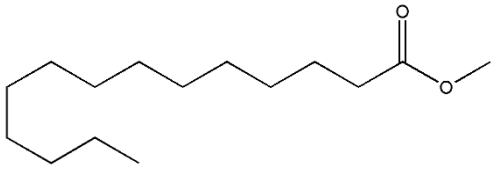

Methyl tetradecanoate (**m/z = 74.00**; Rt = 4.373 mins.; fatty acid methyl esters)

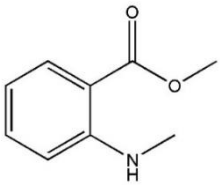

Benzoic acid, 2-(methylamino)-, methyl ester (**m/z = 165**; Rt = 10.595 mins.; benzoic acid esters)

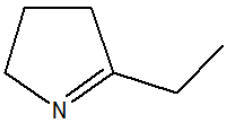

2-Ethyl-1-pyrroline (**m/z = 41.00**; Rt = 5.197 mins.; pyrrole-based alkaloid)

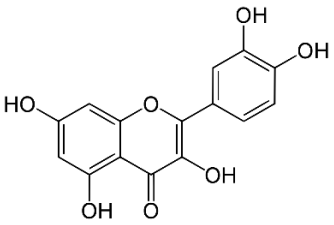

Quercetin (**m/z = 65**; Rt = 5.390 mins.; flavonoid)

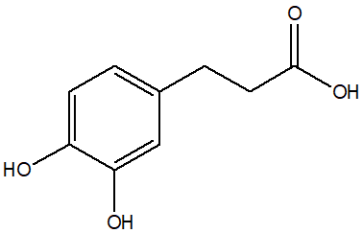

Dihydrocaffeic acid (**m/z = 41**; Rt = 4.945 mins.; phenolic)

Figure 3. The molecular structure of some supposed LmL-based phytochemicals

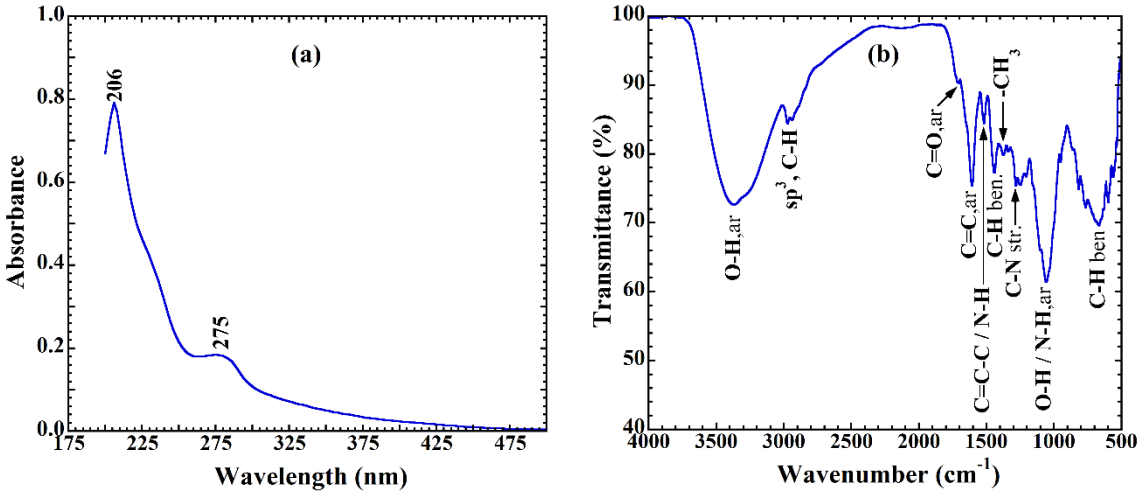

Figure 4. UV-Vis (a) and FTIR (b) spectra of the balk LmL extract

Figure 4b illustrates the functional groups of phytochemicals found in LmL, as determined from the FTIR spectra ranging from 4000 to 500 cm^{-1} wavenumber. The FTIR peaks at 3363 cm^{-1}, 2971 cm^{-1}, and 2945 cm^{-1} correspond to the O–H stretching vibrations of aromatic ring compounds and the asymmetric stretching of C–H vibrations in the conjugated alkanes, respectively (Bhattarai et al., 2021). The presence of aromatic carbonyl (C=O) and C=C functional groups is indicated by weak and strong absorption peaks at 1715 cm^{-1} and 1607 cm^{-1}, respectively.

A sharp absorption peak at 1442 cm^{-1} indicates C–H bending vibrations (scissoring) in the methyl or methylene group. Additionally, a weak peak at 1375 cm^{-1} reveals the bending (deformation) vibration of the $–CH_3$ group (Saifitri et al., 2021). The FTIR peaks at 1282 cm^{-1} and 667 cm^{-1} signify the presence of secondary metabolites with C–N stretching and C–H bending functional groups in aromatic compounds, respectively (Nandiyanto et al., 2023). Moreover, the sharp peak at 1059 cm^{-1} is associated with O–H or C–N bending vibrations in aromatic compounds (Bhattarai et al., 2026).

Investigation on acute oral toxicity (AOT) analysis to assess the environmental safety of the plant extract LmL, using *Albino mice* to examine the effect of the lethal dose (LD50) of both the methanol extract and the dried powder derived from the plant leaves. The study found no mortality in the Albino mice at a single dose level exceeding 2000 mg/kg body weight for both the powder and the LmL extract. It indicates that LmL-based concrete additives do not pose risks to humans and are considered green materials. Consequently, the results from the screening tests, including GC-MS, UV-Vis, FTIR, and AOT analyses, indicate the presence of various functional groups containing heteroatoms such as nitrogen (N) and oxygen (O) in LmL.

It suggests the presence of non-toxic alkaloids, flavonoids, steroids, phenols, resins, glycosides, and saponins in the methanol. These classes of phytochemicals are well known for their corrosion-resistant properties. They demonstrate the maximum inhibition efficiency, mostly due to the presence of heteroatoms (such as O, N) and unsaturated aromaticity, which contribute to the formation of a diffusion-barrier passive layer on the MS surface. These heteroatoms (O or N), unsaturated bonds, or aromatic compounds attach to the corroded MS surface, forming a diffusion-barrier passive film on Fe ions, obstructing the ingress of corrosive ions in simulated concrete systems.

Electrochemical examination on anti-corrosion behavior

The anti-corrosion behavior of LmL-based phytochemicals was investigated on MS rebar in SCPS-IndE using OCP, PDP, CV, and EIS techniques. The OCP value delivers the resilience, anti-corrosion behavior, and surface prerequisites of the anti-corrosive diffusion-barrier film. Figure 5a shows the OCP changes of MS in SCPS-IndE without (control) and with 500-2000 ppm LmL as a function of exposure time. The changes observed in OCP after 60 minutes of exposure provide qualitative information about the anti-corrosion behavior of the LmL extract in the control SCPS-IndE condition, as evidenced by the shift in OCP at -0.245 V vs Ag/AgCl.

In contrast, the OCP exhibited a transition to more noble levels of –0.155 V, –0.118 V, and –0.122 V with increasing LmL concentrations at 500 ppm, 1000 ppm, and 2000 ppm, respectively, as shown in Table 3. Overall, the addition of LmL extract to SCPS-IndE shifts the OCP towards a more noble value, suggesting its role in forming a consolidated and protective layer. It indicates that the MS surface becomes less prone to rapid dissolution. These findings indicate that the LmL extract functions effectively as an anti-corrosive additive in aggressive simulated marine conditions of concrete pore solutions, thereby mitigating corrosion of mild steel.

Figure 5b presents the polarization curve data of MS in environments containing 1000 ppm, 2000 ppm, and 4000 ppm LmL in simulated sulfate-contaminated concrete (SCPS-IndE). It also includes data from the control-SCPS-MarE, which did not contain LmL, to examine the kinetics and efficiency of anti-corrosion behavior on MS rebars. The corrosion potential (OCP) shifted to a more noble (i.e., more positive) direction by more than 85 mV, ranging from 107 mV to 147 mV, compared to the control conditions in the steady-state potential region. Furthermore, the anodic current density (i_{ano}) decreased with increasing concentrations of LmL from 500 to 2000 ppm in SCPS-IndE, as shown in Figure 5b. These findings indicate that LmL-based phytochemicals act as anti-corrosive agents by forming a protective layer on the MS, thereby preventing further dissolution in the highly corrosive sulfate-polluted concrete environment (i.e., SCPS-IndE).

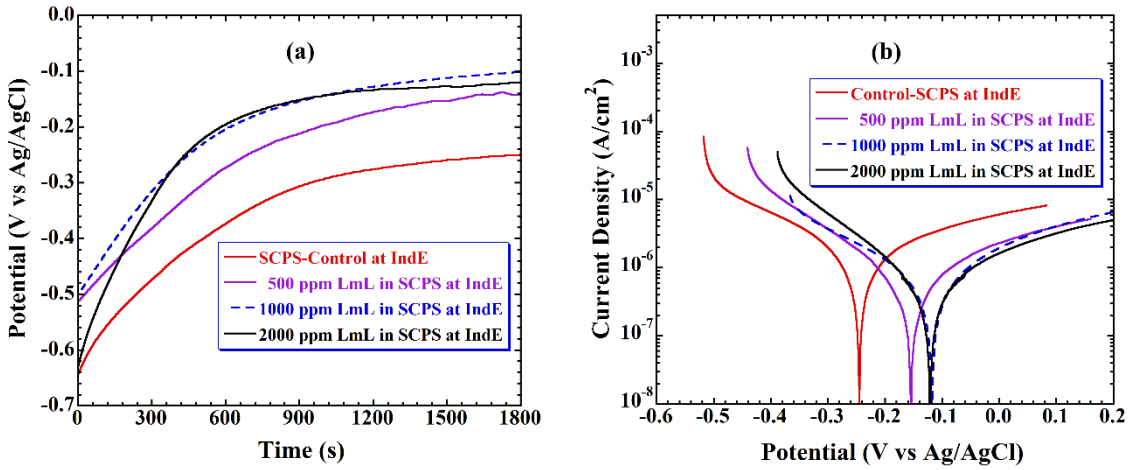

Figure 5. Changes in the OCP (a) and polarization curve (b) of MS in SCPS with 500-2000 ppm LmL and without (control) at IndE condition

The anti-corrosion kinetic properties and efficiency of 500-4000 ppm LmL on the MS in SCPS-IndE are studied based on the corrosion current (i_{corros}) from the Tafel polarization or linear polarization resistance (LR_{pol}) method, using PDP curves from the segment of anodic and cathodic polarization in ± 25 mV from the corrosion potential (OCP). Table 3 summarizes the corrosion rate from i_{corros}, using equation (1), including the Tafel kinetic parameters like OCP, i_{corros}, anodic Tafel slope (β_{anode}), cathodic Tafel slope ($\beta_{cathode}$), and linear polarization resistance (LR_{pol}), using the Stern-Geary equation as in equation (8). The equation (1) is modified for the estimation of corrosion rate of MS based on the experimental value of i_{corros}, as given in equation (9).

$$LR_{pol} = \frac{\beta_{anode} \times \beta_{cathode}}{2.303 \times i_{corros} \times (\beta_{anode}+\beta_{cathode})} \quad \ldots (8)$$

$$\text{Corrosion rate: } i_{corros}\,(\text{mm/y}) = 0.0116 \times i_{corros} \quad \ldots (9)$$

Table 3. Kinetic parameters estimated from Tafel polarization

LmL (ppm)	OCP (V vs Ag/AgCl)	i_{corros} ($\mu A/cm^2$)	β_{anode} (mV/dec)	$-\beta_{cathode}$ (mV/dec)	LR_{pol} ($\Omega.cm^2$)	Corrosion rate (mm/y)	$IE_{icorros}$ (%)
Control	-0.245	0.21792	28.611	34.719	31.254	0.00253	-
500	-0.155	0.08745	14.235	13.461	34.353	0.00101	51.00
1000	-0.118	0.06468	15.576	15.264	51.757	0.00075	70.32
2000	-0.122	0.04409	14.065	15.095	71.700	0.00051	79.77

The slopes of the anodic (β_{anode}) and cathodic ($\beta_{cathode}$) Tafel plots decrease as the concentration of LmL increases from 500 to 2000 ppm in SCPS at IndE condition. This trend suggests that a higher degree of surface coverage is attained through the adsorptive accumulation of LmL-based phytochemicals on the corroded mild steel (MS) surfaces. This accumulation blocks active sites and forms a more uniform passive film on the MS rebars in SCPS, resulting in reduced corrosion (Oghenerukevwe et al., 2026). The interaction of LmL-based phytochemicals with the MS rebar surface occurs through physicochemical adsorption, affecting the charge transfer coefficient. This process lowers the energy required to inhibit surface kinetics, thereby altering the cathodic hydrogen evolution mechanism and anodic metal dissolution pathways, as is characteristic of mixed-type inhibitors. The linear polarization resistance (LRpol), estimated from the Stern-Geary equation (9), is supposed to be inversely proportional to the corrosion rate (Schneck, 2019). It means that as LRpol increases, the corrosion rate decreases. The LRpol value allows for estimating the corrosion rate within a few minutes of polarization without significantly disturbing the system and requiring a small polarization range from the OCP. Hence, it is an effective method for measuring corrosion rates in SCPS-IndE with LmL.

The peak current (I_{peak}) of a cyclic voltammogram (CV) was utilized, except for the polarization (PDP) examination, to investigate the corrosion kinetics and the effects of anti-corrosion efficiency on the MS rebars in SCPS under sulfate-polluted IndE (Fig. 6a, 6b). Addition of 500-2000 ppm LmL in SCPS at IndE, the anodic peak current (I_{peak}) reduced with LmL concentrations, implying the building of a diffusion barrier passive film onto the corroded MS rebar that virtually functions as an anti-corrosion property. The peak current (I_{peak}) of 1.572×10^{-3} A/cm^2 with the addition of 500 ppm LmL from 3.335×10^{-3} A/cm^2 without the addition of extract (i.e., control-SCPS-IndE), but it reduced to 1.355×10^{-3} A/cm^2 and 1.240×10^{-3} A/cm^2 with the addition of 1000 and 2000 ppm LmL, respectively, assuring inhibitive effects of LmL to control corrosion of the MS rebars, exposed in the SCPS at very aggressive IndE conditions. Consequently, the I_{peak}-based anti-corrosion efficiency (IE_{Ipeak}) is estimated about 62.82% at 2000 ppm LmL.

The electrochemical impedance spectroscopy (EIS) is becoming one of the key electrochemical methods (Zulkifli et al., 2022), alongside PDP, CV, mass loss measurements, and surface analysis methods based on adsorption models, for studying the formation of passive films on corroded MS rebar surfaces in the reactive environment of SCPS-IndE. Unlike Tafel slopes, it does not provide direct estimates of corrosion rates. Additionally, constructing an equivalent electrical circuit from EIS data is challenging without prior information. Although EIS allows averaging impedance across the entire surface, it does not effectively capture localized corrosion damage to the passive film. It encounters difficulties when used as a standalone technique for assessing corrosion kinetics, particularly in accurately determining corrosion rates.

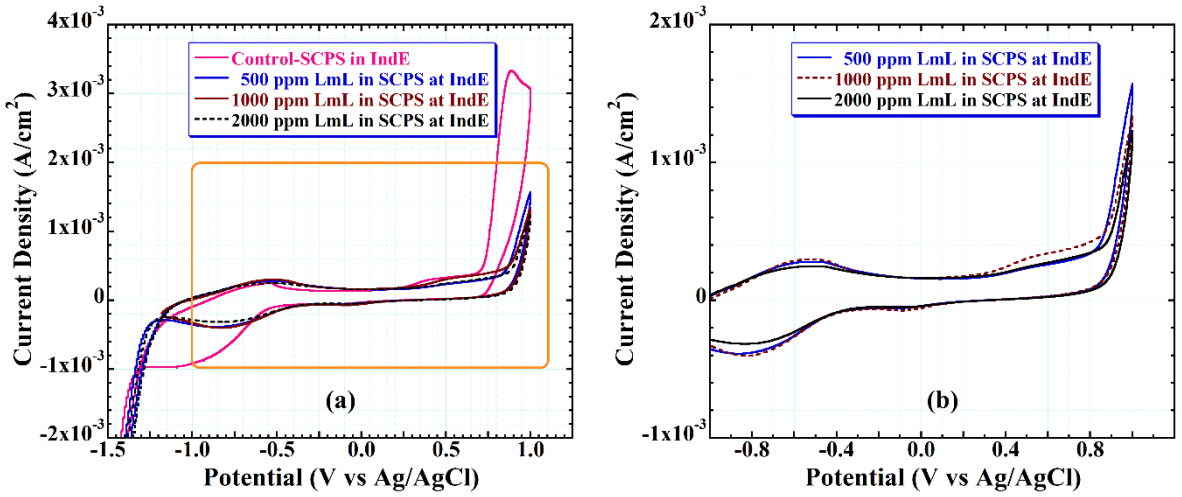

Figure 6. CV curves for MS in SCPS with 500-2000 ppm LmL and without (control) at IndE condition (a) and enlarged curves in 500-2000 ppm LmL (b)

Figure 7a presents the Nyquist plots for the corroded MS rebars in SCPS, treated with 500-2000 ppm LmL, obtained from the EIS investigation. The Nyquist plots, with a standard semicircle with a single capacitive loop, as illustrated in Figure 7(a), are attributed to charge transfer processes on the MS surface. As the concentration of LmL increases, the diameter of the capacitive loop expands. The Nyquist plot analysis helps identify the resistive, capacitive, or diffusive behaviors of an anti-corrosive passive layer formed at the interfacial region between the corroded MS surface and SCPS under the LmL at IndE conditions. In the lower frequency region (the left side of the BMP), the charge transfer resistance (R_{ct}) is indicated by increasing the resistance at higher LmL concentrations, suggesting the development of a high-impedance anti-corrosive layer on the MS rebar specimen. Besides, the R(Q(R(QR))) circuit, as illustrated in Figure 7a, was used to model the EIS data for anti-corrosion behavior of 500-2000 ppm LmL in SCPS-IndE applying the ZSimpWin 3.20 software.

The charge transfer resistance (R_{ct}) increases with the concentrations of LmL, ranging from 500 to 2000 ppm, while the solution resistance (R_s) decreases. Table 4 indicates an increase in the R_{ct} value, rising from 3.080×10^4 Ω cm² for the control-SCPS at IndE to 7.458×10^4 Ω cm² with the addition of 2000 ppm LmL. Hence, the maximum anti-corrosion efficacy observed is 58.7% at 4000 ppm of MaL in SCPS-MarE, based on the R_{ct} values. Additionally, the parameter $\chi^{'2}$, used in the impedance approach, assesses the fitting quality of the selected equivalent circuit [i.e., R(Q(R(QR)))] to evaluate the accuracy of the fitted EIS data. This increase in R_{ct} values may be due to the adsorption of active phytocompounds from LmL at the interface between MS and SCPS-IndE. The adsorption process could impede charge transfer at the MS/SCPS-IndE solution interface, leading to enhanced corrosion inhibition.

The analysis of the Bode plots reveals substantially high phase angle values with 500-2000 ppm LmL, as illustrated in Figure 7(b), which approximates a considerable reduction in surface roughness in the presence of the LmL-based phytochemicals, attributing to the development of a shielding surface film. The log(Z) versus log(f) plot, also known as the Bode magnitude plot (BMP), shown in Figure 7(b), is used to analyze how the total impedance magnitude transitions from high to low frequency ranges (specifically from 10^4 to 10^{-2} Hz). The intermediate frequency region (the middle section) of the BMP exhibits linear slopes within the 10^2 to 10^{-2} Hz frequency range, with slopes between –0.70 and –0.72, indicating capacitive behavior similar to that of the double-layer capacitance (C_{dl}), which is attributed to surface roughness or heterogeneity.

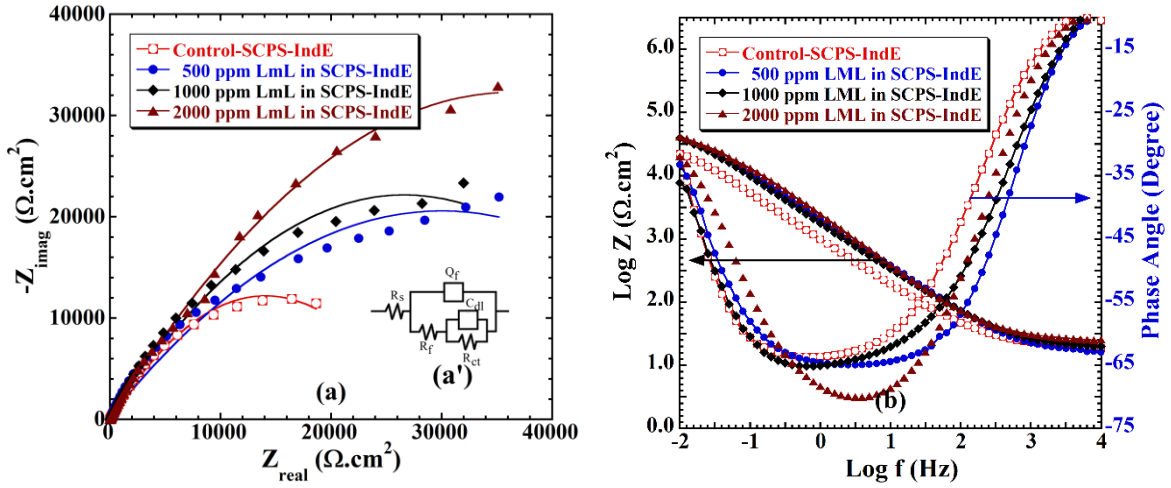

Figure 7. Nyquist (a) and Bode (b) plots for MS rebar in control-SCPS and SCPS with 500-2000 ppm LmL at simulated sulfate polluted industrial (IndE) condition

Table 4. Impedance parameters of MS in SCPS-IndE with different concentrations of LmL at 30 °C

LmL (ppm)	R_s (Ω cm^2)	$Q_f \times 10^{-5}$ (S sec^n cm^{-2})	n_f	$R_f \times 10^4$ (Ω cm^2)	$C_{dl} \times 10^{-5}$ (S sec^n cm^{-2})	n_{dl}	$R_{ct} \times 10^3$ (Ω cm^2)	χ'^2	IE_{Rct} (%)
Control	14.88	9.072	0.7724	3.798	1.521	0.2364	1.185	0.002607	-
500	24.13	9.794	0.7850	4.983	2.736	0.1624	2.932	0.014530	59.58
1000	16.15	11.80	0.7551	10.24	2.591	0.0799	3.495	0.008684	66.09
2000	16.07	12.13	0.7497	6.879	3.157	0.4712	50.09	0.005256	97.63

The maximum phase angle peak exhibits a slight increase with LmL concentrations in SCPS under IndE conditions, as presented in Figure 7b. It is important to observe that the phase angle approaches nearly –71°, indicating strong passivation performance. The high phase angles observed at elevated frequencies for the MS samples exposed in SCPS with increasing LmL concentrations at IndE indicate an enhanced corrosion inhibition compared to the control sample. It suggests that this system demonstrates superior capacitive performance. The differences observed in the results from the EIS analysis have a significant inhibitory effect of LmL on MS in SCPS-IndE. The effect of LmL concentrations is attributable to a larger presence of corrosion-inhibiting phytochemicals in the sulfate-polluted SCPS-IndE condition. These phytochemicals likely enhance anti-corrosion efficiency on the MS surface by effectively blocking the pathways through which aggressive ions can reach it.

Anti-corrosion efficiency and adsorption kinetics of phytochemicals

The outlines of the anti-corrosion efficiency of LmL-based phytochemicals on MS rebars in SCPS at IndE from the different electrochemical investigations (i.e., OCP, PDP, CV, and EIS) suggest that the LmL-derived phytochemicals enhanced to form a corrosion-resistant protective layer by adsorption phenomena onto the MS surface that prevents the active dissolution in sulfate-polluted concrete environments, thereby mitigating the destructive impact of MS rebars. The adsorption phenomena of the LmL-based phytochemicals are investigated using four mathematical isotherm models (i.e., Langmuir, Temkin, El-Awady, and Freundlich), which illustrate how plant-based phytochemicals interact with the MS surface to form an anti-corrosive passive layer, enhancing anti-corrosion efficiency. This layer enhances anti-corrosion efficiency, as indicated by the estimated corrosion current density (i_{corros}) calculated from the Tafel slope, as discussed in the previous section. By employing equations (2) and (3), as described in the experimental section of the manuscript, we estimated the anti-corrosion efficiency (IE) based on the icorros ($IE_{icorros}$) and surface coverage (θ), respectively, and also other relevant parameters, as summarized in Table 5.

Table 5. Kinetic parameters estimated from Tafel polarization

C_{LmL} (ppm)	i_{corros} (μA/cm^2)	$IE_{icorros}$ (%)	θ	C_{LmL} / θ (ppm)	Log C_{LmL} (ppm)	Log(θ/1-θ)	Log θ
Control	0.21792	-	-				
500	0.08745	51.00	0.5100	980.39	2.699	0.01738	-0.2924
1000	0.06468	70.32	0.7032	1422.0	3.000	0.37464	-0.1529
2000	0.04409	79.77	0.7977	2507.3	3.301	0.59575	-0.0982

Increasing the concentration of LmL in SCPS-IndE significantly reduces the corrosion current density (i_{corros}) of mild steel (MS) from 21.792×10^{-2} μA/cm² in the control group to 4.409×10^{-3} μA/cm² at 2000 ppm LmL. It also enhances the anti-corrosion efficiency ($IE_{icorros}$) from 51.00% at 500 ppm LmL to 79.77% at 2000 ppm LmL, as shown in Figs. 8(a) and 8(b). These improvements are attributed to the increased adsorption of LmL-based phytochemicals at the electric interfacial regions of the corroded MS rebars and SCPS-MarE as the concentration of the plant extract rises to 2000 ppm.

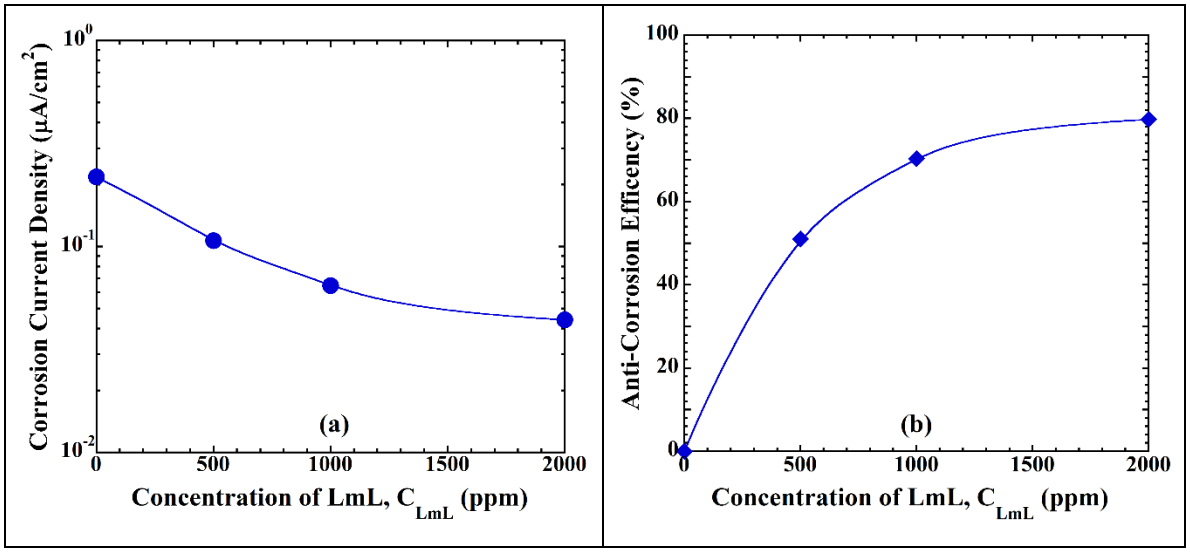

Figure 8. The changes in corrosion current density (icorros) (a) and anti-corrosion efficiency (b) of 1000-4000 ppm MaL on MS in SCPS at MarE environments

Such anti-corrosion efficacy at a high concentration of 2000 ppm LmL typically indicates that the adsorption sites on the corroded MS surface are nearing saturation. According to adsorption isotherm models, the corroded MS surface has a limited number of sites for the adsorption of LmL-based phyto-molecules at 2000 ppm. As the concentration increases from 500 ppm to 1000 ppm, these phyto-molecules occupy the available free sites, leading to a significant rise in efficiency from 51.00% to 70.32%. However, when the concentration reaches 2000 ppm, most corroded sites are covered, resulting in a plateau where further increases in concentration do not enhance effectiveness. To analyze this, we typically fit the experimental data to an adsorption isotherm model, such as the Langmuir adsorption isotherm. This model will demonstrate that the phyto-molecules are forming a protective monolayer on the surface of MS, as discussed in the following section of this manuscript.

The results suggest that LmL-based phytochemicals adhere to the surface of MS, creating a protective layer that hinders the penetration of corrosive sulfate ions, thus reducing their damaging effects on the concrete system. Specifically, the anti-corrosion efficiency ($IE_{icorros}$) of a 2000 ppm leaf extract from *Ziziphus budhensis* was 73.6%, while *Tagetes erecta* exhibited 58.4% (Gautam et al., 2024). Other plant extracts, including *Elaeocarpus angustifolius* Blume (Gautam et al., 2025b), *Melia azedarach* (Bhattarai et al., 2026b), and *Sesamum indicum* (Gautam et al., 2025a), demonstrated 73.4%, 77.5%, and 77.4% $IE_{icorros}$, respectively, in SCPS under different corrosive conditions. This study found that 2000 ppm of LmL in SCPS under IndE exposure exhibited an anti-corrosion efficiency of 79.77%. This finding supports the concept that LmL possesses compelling corrosion-resistant properties for mild steel rebars in SCPS, even under aggressive sulfate-polluted environments, outperforming other plant-based phytochemicals by forming corrosion-resistant passive layers, as explained by adsorption isotherm models subsequently.

Among the various adsorption isotherm models, the Langmuir model is one of the simplest, most widely recognized, and effective practical approaches. This model describes the formation of a monolayer of adsorbed plant-based phytochemicals on a uniform metal surface, showing high anti-corrosion efficiency. Figure 9(a) illustrates a straight-line Langmuir plot, which is created by plotting C_{LmL}/θ values against C_{LmL}. A slope and coefficient of determination (R^2) of the plot are approximately 0.9892 and 0.9925, respectively, as illustrated in Figure 9a and in Table 6. It demonstrates how well the adsorption of LmL-based phytocompounds onto the corroded MS surface in SCPS at IndE can be analyzed using a dimensionless separation factor (R_L) derived from the Langmuir isotherm equation: $R_L = 1 / (1 + K_{L\text{-}ads} \times C_{LmL})$, as described elsewhere (Mamudu et al., 2023). In the present case, R_L is less than 1 (between 0.23 and 0.55), which suggests favorable adsorption of LmL-based phytochemicals on the MS surface.

Similarly, a linear Temkin plot, as shown in Figure 9b, has an R^2 value of 0.9622, indicating that the Temkin linear plot fits less well than the Langmuir plot. This

model illustrates the interactions between corroded MS and the adsorbing LmL-based phytochemicals, providing insights into surface heterogeneity and homogeneity. Based on the slope of the Temkin isotherm plot (0.55105), the value of the interaction factor (*f*) between phytochemical molecules is –4.1776 (see Table 6), suggesting that the adsorbed LmL-based phytochemicals exert a repulsive force due to the negative *f* value. This repulsive force facilitates the formation of a monolayer of the LmL extract on the corroded mild steel surfaces, as indicated by the Langmuir adsorption model. This behavior of a monolayer formation on the MS is also consistent with the El-Awady adsorption isotherm model.

As shown in Figure 9c, the El-Awady adsorption plot is not as well-fitted as the Langmuir plot, with an R^2 value of 0.9778 and a slope of 1.05 (i.e., *y* constant). It indicates that the monolayer of phytochemical molecules occupies more than one active site on the corroded MS rebar surface in SCPS at concentrations ranging from 500 to 2000 ppm under IndE conditions. Besides, the closer the *y* constant of the El-Awady plot is to one (Table 6), the narrower the distribution of adsorption energy becomes, forming a more homogeneous passive film formed by the adsorption of LmL-based phytomolecules. This process leads to the formation of a homogeneous monolayer passive film, as suggested by both the Temkin and Langmuir models (El-Awady et al., 1992).

.

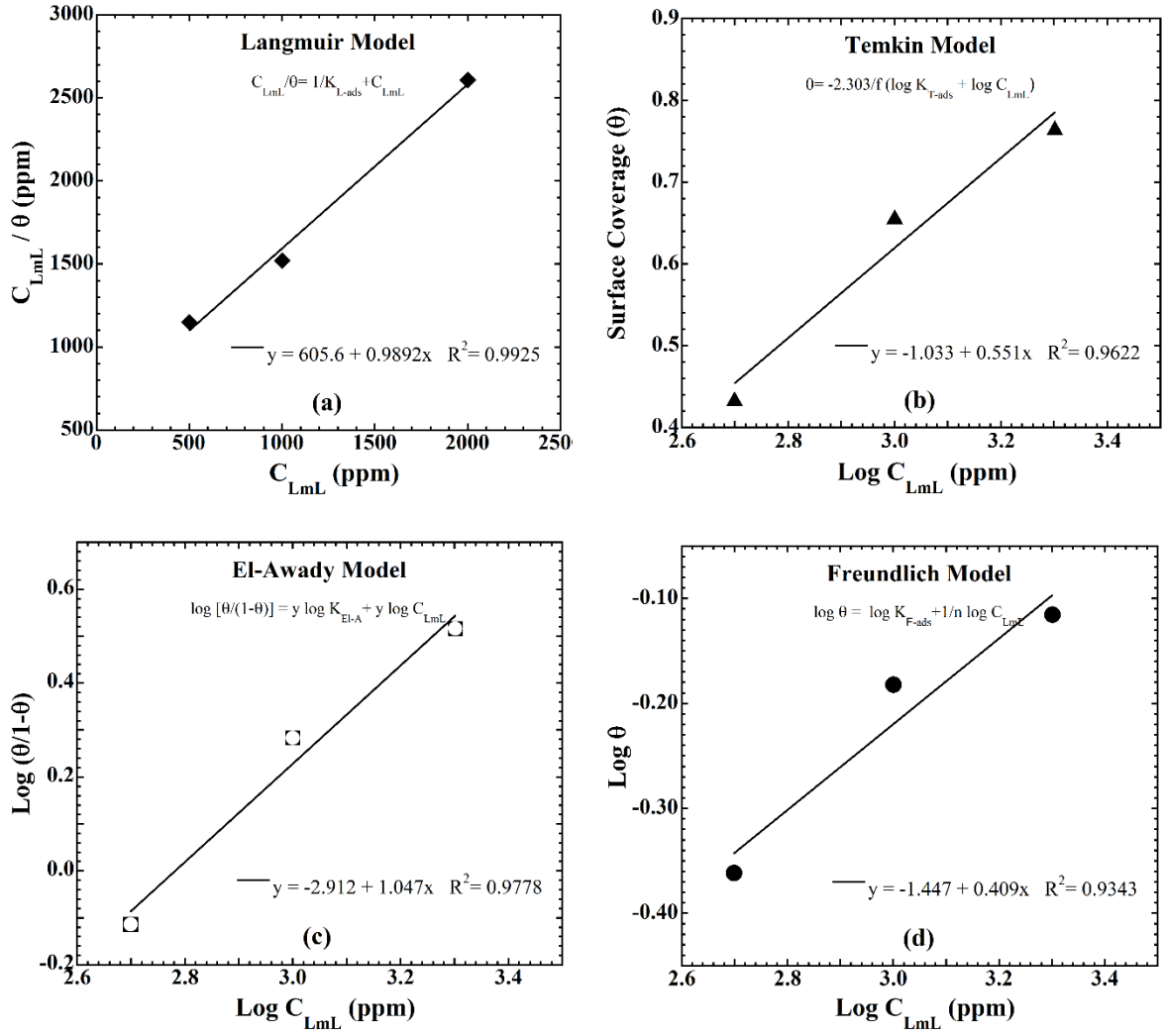

Figure 9. Langmuir (a), Temkin (b), El-Awady (c), and Freundlich (d) adsorption plots, elucidating the properties for passive film formation on MS in SCPS with LmL-phytochemicals under IndE condition

Besides the above-discussed adsorption isotherm models, the Freundlich model illustrated the adsorption power of the LmL-based phyto-compounds onto the MS, as exemplified in Figure 9d. Figure 9d and Table 6 clearly indicate that the Freundlich linear plot has a slope (1/n) of 0.4090, which is significantly less than one, even though it fits less (i.e., R^2= 0.9343) than the other three isotherm models discussed at this time. It suggests a favorable adsorption of LmL-based phytochemicals on the MS surface in SCPS at IndE, accompanied by a high adsorption heat. This statement is in harmony with the projection of monolayer passive film formation on the corroded MS surface in the sulfate-polluted concrete system with sufficient adsorption energies from the Langmuir, Temkin, and El-Away models. Overall, these isotherm models could successfully evaluate the anti-corrosion efficiency mechanism of LmL onto corroded MS in SCPS at IndE condition through the formation of corrosion-resistant monolayer passive film at the interfacial regions between the concrete electrolyte and the corroded MS rebars

Table 6. Adsorption parameters derived from different isotherm models

Models	R^2	Slope	R_L	f	1/y	n
Langmuir	0.9925	0.9892	0.23-0.55	–	–	–
Temkin	0.9622	0.5510	–	-4.18	–	–
El-Awady	0.9369	1.047	–	–	1.047	–
Freundlich	0.9343	0.409	–	–	–	2.44

Anti-corrosion mechanism of LmL-phytocompounds

Based on the previous discussions in this manuscript, the anti-corrosion mechanism of LmL-based phytocompounds on exposed mild steel (MS) rebars in sulfate-polluted, simulated concrete pore solution (SCPS-IndE) is an effective and sustainable approach for corrosion prevention. This process involves three key steps, characterized by the physicochemical interactions of phyto-compounds, such as flavonoids, alkaloids, tannins, carboxylic acids, and phenolic acids, with the corroded surface of the MS, as reported in prior studies (Bensouda et al., 2019; Bhattarai et al., 2026a).

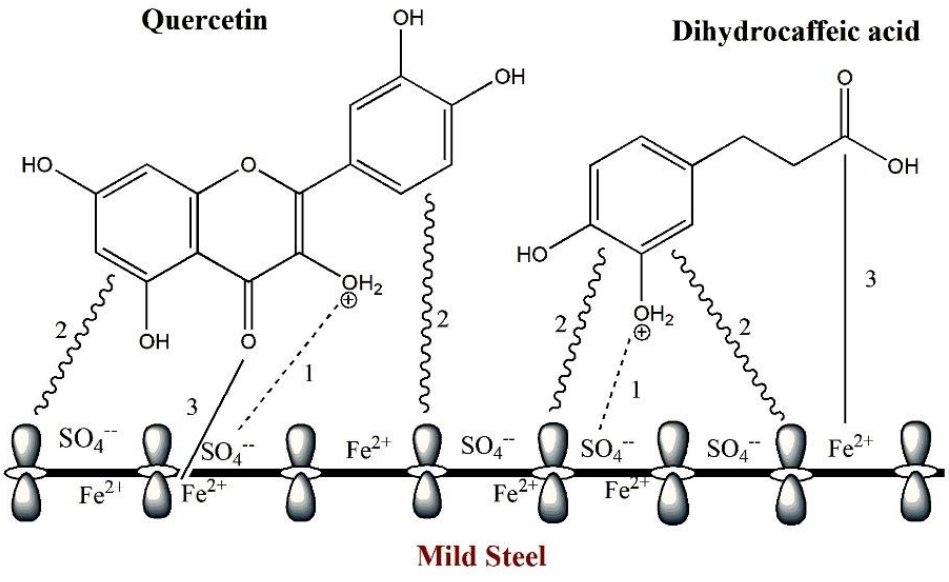

Figure 10. Diagrammatic sketch of the anti-corrosion adsorption mechanism of phytomolecules on the mild steel in sulfate-contaminated concrete pore solution

1. *Physical Adsorption of Protonated Phytochemicals*: To initiate the adsorption mechanism of phytomolecules, it is crucial to understand how the surface charge of MS rebars develops in sulfate-contaminated SCPS under industrial conditions (IndE). The surface charge of MS arises only under zero charge potential conditions, where the open circuit potential (OCP) minus the equilibrium potential (EQP) equals zero, as reported by Schweinsberg and Ashworth (1988). The EQP of iron is −1 V vs Ag/AgCl in concentrated alkaline solutions with a pH of 12.5 or higher (Amaral & Muller, 1999), which is significantly less noble than the OCP of the MS rebar in present study. In our research, the OCP of the MS rebar is recorded at −0.242 V vs Ag/AgCl in strongly alkaline SCPS under sulfate contamination, resulting in a positively charged surface on the MS rebar, as the difference between OCP and EQP was +0.758 V (i.e., -0.242 +1.0 = 0.758 V), significantly greater than zero. Consequently, aggressive ions like SO_4^{2-} adsorb on the positively charged surface through physical adsorption, followed by the adsorption of protonated LmL-phytochemicals via coulombic forces, as illustrated in Figure 10 (dotted lines). This process enhances for the formation of anti-corrosive layer on MS in the SCPS-IndE system.
2. *Chemical Adsorption by Coordination Bonding*: Next step, the chemical adsorption occurs through coordination bonding between the non-bonding electrons of heteroatoms (like oxygen and nitrogen) in LmL-based phytochemicals and vacant d-orbitals of iron atoms (Verma et al., 2026). It forms a durable protective layer at the interface of the corroded MS rebar surface and the SCPS-IndE electrolyte, preventing corrosion by blocking corrosive ions and altering the surface chemistry.
3. *Chemical Adsorption by Retro-donation vice versa Interaction*: Chemical adsorption may occur through retro-donation or donor-acceptor interactions between the d-electrons of Fe atoms and the empty antibonding orbitals of phytochemicals from LmL extracts in the next step of the anti-corrosion efficiency mechanism, as shown in Figure 10.

CONCLUSION

This study presents the first application of a methanol extract from the leaves of *L. monopetala* (Roxb) Pers (denoted as LmL) as an anti-corrosive additive in a simulated concrete system. The LmL extract enhances the corrosion resistance of MS rebar in the highly alkaline environment of SCPS-IndE with 0.5 moles of sulfate. The analysis employs electrochemical methodologies, including OCP, PDP, CV, and EIS, alongside adsorption models. The research employed techniques such as UV-Visible spectroscopy, FTIR, GC-MS, and chemical analysis, including toxicity tests, to characterize the LmL extract.

Investigations have demonstrated that phytochemicals derived from LmL exhibit superior anti-corrosion properties on MS in SCPS-IndE at 30 °C. The effectiveness of these LmL-based phytochemicals, comprised of alkaloids, flavonoids, phenolic compounds, and conjugated substances, aligns with findings from various screening, spectrophotometric, and chromatographic analyses, which function as initiators for the construction of a diffusion barrier passive film to diminish the corrosion threat of the MS rebars in SCPS-IndE with 500-2000 ppm LmL.

The maximum anti-corrosion efficiency achieved are 79.77% (i_{corros}-base from PDP), 62.82% (I_{peak}-base from CV), and 97.63% (R_{ct}-base from EIS) with the addition of 2000 ppm LmL to SCPS-IndE at 30 °C, indicating the formation of an adsorption passive film, effectively represented by the Langmuir adsorption model, including three other adsorption isotherm models. The PDP demonstrates that the LmL functions as a mixed-type inhibitor on the surface of MS in SCPS-IndE. This research, first reported, encourages material scientists to examine Nepali plant-based extracts as concrete additives on an industrial scale, aiming to replace the more toxic and less effective synthetic waterproofing agents used in concrete.

ACKNOWLEDGMENTS

Authors acknowledged to P. Venkatesh Rajaraman and Madhab Gautam of Department of Chemical Engineering -IIT Guwahati, India, for electrochemical measurement.

AUTHORS CONTRIBUTION

Conceptualization: NPB, JB; Methodology: RT, YP; Validation: JB; Investigation: RT, KTKM, UP, YP; Data analysis: DBS, NPB, JB; Writing-original draft: NPB, JB; Writing-review & editing: JB, NPB; Supervision: JB; Funding acquisition: DBS

FUNDING

University Grants Commission, Nepal (PhD-81/82-S&T-08).

ORCIDs

Jagadeesh Bhattarai:

https://orcid.org/0000-0003-0058-079X

CONFLICT OF INTEREST

Authors proclaim that they have no competing claims.

DATA AVAILABILITY STATEMENT

Upon demand, the corresponding author will supply supporting data.

SUPPLEMENTARY INFORMATION

None

REFERENCES

Alemnezhad, M.M., Ghaffarinejad, A., & Omidali, F., 2023. White turnip bark extract as a new green and cost-effective corrosion bio-inhibitor for carbon steel in 1M HCl solution: Experimental and theoretical studies. *Chemical Physics Letters*, *831*, 140855. https://doi.org/10.1016/j.cplett.2023.140855

Alvarez, L.X., de Rincón, O.T., Escribano, J., & Rincon Troconis, B.C. (2023). Organic compounds as corrosion inhibitors for reinforced concrete: a review. *Corrosion Reviews*, *41*(6), 617–634. https://doi.org/10.1515/corrrev-2023-0017

Amaral, S.T., & Müller, I.L. (1999). Passivation of pure iron in alkaline solution containing silicate and sulphate-galvanostatic and potentiostatic studies. *Corrosion Science*, *41*(4), 747–758. https://doi.org/10.1016/S0010-938X(98)00148-6

Amgain, K., Subedi, B.N., Joshi, S., & Bhattarai, J. (2022). A comparative study of the anticorrosive response of *tinospora cordifolia* stem extract for al and cu in biodiesel-based fuels. *E3S Web of Conferences*, *355*, 01005. https://doi.org/10.1051/e3sconf/202235501005

Arifuzzaman, S., Labu, Z.K., Ani, B.D., Karim, S., & Rahman, M.T. (2025). Methanolic crude extract of *Litsea monopetala* leaves combats oxidative stress, clot formation, inflammation and stool frequency in animal model. *PLoSOne*, *20*(5), e0313706. https://doi.org/10.1371/journal.pone.0313706

Arya, E.K., Dhanya, B.S., 2020. Corrosion control of reinforced concrete structures in construction industry: A review. *IOP Conference Series: Material Science and Engineering*, *1114*, 012006. https://doi.org/10.1088/1757-899X/1114/1/012006

Bensouda, Z., El Assiri, E.H., Sfaira, M., Touhami, M.E., Farah, Abdellah, & Hammouti, B. (2019). Extraction, characterization and anticorrosion potential of an essential oil from orange zest as eco-friendly inhibitor for mild steel in acidic solution. *Journal of Bio- and Tribo-Corrosion*, *5*, 84. https://doi.org/10.1007/s40735-019-0276-y

Bhattarai, J. (2010). *Frontiers of Corrosion Science* (1st ed.), Kshitiz Publication, Kirtipur, Nepal, p. 304.

Bhattarai, J., Gautam, M., & Bhattarai, J. (2026). Tailoring of Nepal-sourced plant extracts as anti-corrosive additives for mitigating rebar corrosion in reinforced concrete beam. *Arabian Journal of Chemistry*, in press.

Bhattarai, J., Somai, M., Acharya, N., Giri, A., Roka, A., & Phulara, N. (2021). Study on the effects of green-based plant extracts and water-proofers as anti-corrosion agents for steel-reinforced concrete slabs. *E3S Web of Conferences*, *302*(1), 02018. http://dx.doi.org/10.1051/e3sconf/202130202018

Dhungana, J.R., Gautam, M., Subedi, D.B., Bhattarai, N.P., & Bhattarai, J. (2025). Exploration of plant-based leaf extracts as anti-corrosive concrete admixtures for extending the service life of reinforcement concrete infrastructures. *E3S Web of Conferences 679*, 01020. https://doi.org/10.1051/e3sconf/202567901020

El-Awady, A.A., Abd-El-Nabey, B.A., & Aziz, S.G. (1992). Kinetic-thermodynamic and adsorption isotherms analyses for the inhibition of the acid corrosion of steel by cyclic and open-chain amines. *Journal of Electrochemical Society*, *139*(8), 2149–2154. https://doi.org/10.1149/1.2221193

Fernandes, C. M., Fagundes, T. D. S. F., dos Santos, N. E., Rocha, T. S. D. M., Garrett, R., Borges, R. M., Muricy, G., Valverde A. L., & Ponzio, E. A. (2019). *Ircinia strobilina* crude extract as corrosion inhibitor for mild steel in acid medium. *Electrochimica Acta*, *312*, 137–148. https://doi.org/10.1016/j.electacta.2019.04.148

Gautam, M., Bhattarai, N.P., & Bhattarai, J. (2024). Leaf-based extracts of Nepal origin plants as efficient inhibitors for controlling rebar corrosion in concrete pore solution. *International Journal of Corrosion and Scale Inhibition*, *13*(4), 2087–2111. http://dx.doi.org/10.17675/2305-6894-2024-13-4-10

Gautam, M., Bhattarai, N.P., & Bhattarai, J. (2025a). *Sesamum indicum* leaf extract as environmentally benign inhibitor to mitigate mild steel corrosion in cement pore solution. *Journal of Institute of Science and Technology*, *30*(1), 101–113. https://doi.org/10.3126/jist.v30i1.74723

Gautam, M., Subedi, D.B., Dhungana, J.R., Bhattarai, N.P., & Bhattarai, J. (2025b). Utilization of bark extract of *Phyllanthus emblica* as a sustainable corrosion inhibitor to reinforced concrete infrastructures in aggressive environments, *E3S Web of Conferences*, *610*, 03002. https://doi.org/10.1051/e3sconf/202561003002

Harb, M.B., Abubshait, S., Etteyeb, N., Kamoun, M., & Dhouib, A. (2020). Olive leaf extract as a green corrosion inhibitor of reinforced concrete contaminated with seawater. Arabian Journal of Chemistry, 13(3), 4846–4856. http://dx.doi.org/10.1016/j.arabjc.2020.01.016

Holla, B.R., Mahesh, R., Manjunath, H.R., & Anjanapura, V.R. (2024). Plant extracts as green corrosion inhibitors for different kinds of steel: A review. *Heliyon*, *10*(14), e33748. https://doi.org/10.1016/j.heliyon.2024.e33748

Hossain, M.S., Aziz, M.T., Sumon, K.M.A., Ibrahim, M., Sultana, A., Sarker, N.G., Das, P., Rahman, M.M., Islam, M.J., & Mohammad Hasem Babu, M.H. (2017). A Study on *Litsea monopetala* for evaluation of pharmacological activities. *Saudi Journal of Medical and Pharmaceutical Sciences*, *3*(8), *873–880.* https://doi.org/10.36348/sjmps.2017.v03i08.012

Iskhakov, I., & Ribakov, Y. (2021). Structural phenomenon based theoretical model of concrete tensile behavior at different stress-strain conditions. *Journal of Building Engineering*, *33*, 101594. https://doi.org/10.1016/j.jobe.2020.101594

Jabed, A., Tusher, M.M.H., Shuvo, Md.S.I., & Imam, A. (2023). corrosion of steel rebar in concrete: A review. *Corrosion Science and Technology*, *22*(4), 272–286. https://doi.org/10.14773/cst.2023.22.4.273

Jagadesh, P., Juan-Valdés, A., Guerra-Romero, M. I., Morán-del Pozo, J. M., García-González, J., & Martínez-García, R. (2021). Effect of design parameters on compressive and split tensile strength of self-compacting concrete with recycled aggregate: An overview. *Applied Sciences*, *11*(13), 6028. https://doi.org/10.3390/app11136028

Jianxia, S., (2012). Durability design of concrete hydropower structures. *Comprehensive Renewable Energy*, *6*, 377–403. https://doi.org/10.1016/B978-0-08-087872-0.00619-3

Kamal, M.S., Ashrafi, S., Sultana, S., A Rashid, M., Ahsan, M., Masud, M.M., & Haque, M.R. (2024). Isolation and characterization of polyprenols from *Litsea monopetala* (Roxb.) Pers. *Dhaka University Journal of Pharmaceutical Sciences*, *23*(1), 63–68. https://doi.org/10.3329/dujps.v23i1.74095

Katuwal, P., Regmi, R., Joshi, S., & Bhattarai, J. (2020). Assessment on the effective green-based nepal origin plants extract as corrosion inhibitor for mild steel in bioethanol and its blend. *European Journal of Advanced Chemistry Research*, *1*(5), 1–12. https://doi.org/10.24018/ejchem.2020.1.5.16

Keles, B., Bakhytzhan, A., Karashina, A., & Nurakhova, A. (2023). Identifying the influence of expanded clay concrete based on a binder from phosphorus slag on the strength of structures from leaked concrete. *Eastern-European Journal of Enterprise Technologies*, *4*(6), 51–58. http://dx.doi.org/10.15587/1729-4061.2023.285183

Khanal, S., & Bhatt, B. D. (2020). Study on the biological activity of *Litsea monopetala* from Panchthar district of Nepal. *Journal of Institute of Science and Technology*, *25*(2), 113–118. https://doi.org/10.3126/jist.v25i2.33747

Labu, Z.K., Karim, S., Akter, R., Arifuzzaman, S., Hassan, Md. H., Hasan, Md. N., Rahman, A., Rahman, Md. T., & Akhtar, A. (2026). Unlocking the phytochemical contents and therapeutic potential of *Litsea monopetala* leaves: Hypoglycemic and antibacterial activities. *Pharmacological Research-Natural Products*, *10*, 100527. https://doi.org/10.1016/j.prenap.2026.100527

Lai, P.F.H., & Sun, T.C. (2017). Optimizing extraction process and characterization of antioxidant ingredients from *Chlorella sorokiniana*. *MOJ Food Processing & Technol*ogy, *5*(1), 202–210. https://doi.org/10.15406/mojfpt.2017.05.00114

Li, K., Zhang, D., Li, Q., & Fan, Z., 2019. Durability for concrete structures in marine environments of hzm project: Design, assessment and beyond. *Cement and Concrete Research*, 115, 545–558. https://doi.org/10.1016/j.cemconres.2018.08.006

Mamudu, U., Alnarabiji, M.S., & Lim, R.C. (2023). Adsorption isotherm and molecular modeling of phytoconstituents from *dillenia suffruticosa* leaves for corrosion inhibition of mild steel in 1m hydrochloric acid solution. *Results in Surfaces and Interfaces*, *13*, 100145. https://doi.org/10.1016/j.rsurfi.2023.100145

Mauro, A.C., Ribeiro, B.D., Garrett, R., Borges, R.M., da Silva, T.U., de Paula Machado, S., de Araujo, J.R., de Oliveira Massafra, S., de Oliveira Junior, F.O.R., & D'Elia, E. (2021). *Ziziphus joazeiro* stem bark extract as a green corrosion inhibitor for mild steel in acid

medium. *Processes*, *9*, 1323. https://doi.org/10.3390/pr9081323

Mohd Azhar, M.A., & Wan Aalleh, W.M.N.H. (2020). Chemical composition and biological activities of essential oils of the genus *Litsea* (Lauraceae) – A Review. *Agriculturae Conspectus Scientificus*, *85*(2), 97–103. https://www.cabidigitallibrary.org/doi/pdf/10.5555/20203225753

Nandiyanto, A.B.D., Ragadhita, R., & Fiandini, M. (2023). Interpretation of fourier transform infrared spectra (FTIR): A practical approach in the polymer/plastic thermal decomposition. *Indonesian Journal of Science & Technology*, *8*(1), 113–126. https://doi.org/10.17509/ijost.v8i1.53297

OECD (2022). *Test No. 425: Acute Oral Toxicity: Up-and-Down Procedure*, OECD guidelines for the testing of chemicals, Section 4, OECD Publishing, Paris. https://doi.org/10.1787/9789264071049-en

Oghenerukevwe, P.O., Onyiriuka, F., Adepoju, T.F., Enomah, S., Mundu, M.M., Muhammed, N., Aisha, N., Usen, I.U., & Oghenejabor, O.D. (2026). Regression analysis of corrosion inhibition of $42CrMo_4$ steel: A case study of acidified large *Maradol* leaf extract, kinetic, thermodynamics, adsorptions, and process parameter optimization. *South African Journal of Chemical Engineering*, *55*, 518–530. https://doi.org/10.1016/j.sajce.2025.12.016

Pandey, N., Gautam, M., Gupta, L., Bhattarai, J., & Bhattarai, N.P. (2024). An inhibitory prospect of leaf extracts of flossflower and yam for rebar steel corrosion in concrete aggregates. *E3S Web of Conference*, *559*, 02008. https://doi.org/10.1051/e3sconf/202455902008

Phulara, N.R., & Bhattarai, J. (2019). Assessment on corrosion damage of steel reinforced concrete structures of Kathmandu valley using corrosion potential mapping method. *Journal of Institute of Engineering*, *15*(2), 45–54. https://doi.org/10.3126/jie.v15i2.27640

Rana, M., Joshi, S., & Bhattarai, J. (2017). Extract of different plants of Nepalese origin as green corrosion inhibitor for mild steel in 0.5 M NaCl solution. *Asian Journal of Chemistry*, *29*(5), 1130–1134. https://doi.org/10.14233/ajchem.2017.20449

Roka, A., Gautam, M., Giri, A., Bhattarai, N.P., & Bhattarai, J., 2023. The anti-degradation consequences of water repellent-based inhibitors for controlling mild steel corrosion in concrete composite. *E3S Web of Conferences*, *455*, 01002. https://doi.org/10.1051/e3sconf/202345501002

Rutsa, V., Yimchunger, A.K., Sangtam, T., Venuh, V., Longkumer, L., Letro, L., Hellen, T.N., Aier, A., & Singh, A. (2026). Plant extracts as environmentally benign corrosion inhibitors in protecting metals from acid media: A review. *Chemical Paper*, *80*, 1–17. https://doi.org/10.1007/s11696-026-04684-x

Sahoo, S., Khan, H. A., Kar, D. M., Pattanaik, S., & Rath, D. (2024). LC-QTOF-MS/MS metabolic profiling and hepatoprotective effects of *Litsea monopetala* bark methanol extract against liver injury in rats and HepG2 cells: Hepatoprotective Potency of *Litsea monopetala*. *Cellular and Molecular Biology*, *70*(9), 156–169. https://doi.org/10.14715/cmb/2024.70.9.22

Saifitri, E., Humaira, H., Nazaruddin, N., Susilawati, S., Murniana, M. & Md Sani, N.D. (2021). *Dioscorea alata* L. anthocyanin extract as methanol as a sensitive pH active compound. *Journal of Physics Conference Series*, *1869*(1), 012508. http://dx.doi.org/10.1088/1742-6596/1869/1/012058

Schneck, U. (2019). Insights from corrosion current measurements on corrosion mechanisms in reinforced concrete and on the evaluation of other corrosion data. *MATEC Web of Conferences*, *289*, 03008. https://doi.org/10.1051/matecconf/201928903008

Schweinsberg, D.P., & Ashwortht, V. (1988). The inhibition of the corrosion of pure iron in 0. 5 m sulfuric acid by n-alkyl quaternary ammonium iodides. *Corrosion Science*, *28*(6), 539–545. https://doi.org/10.1016/0010-938X(88)90022-4

Subedi, B.N., Amgain, K., Joshi, S., & Bhattarai, J. (2019). Green approach to corrosion inhibition effect of *vitex negundo* leaf extract on aluminum and copper metals in biodiesel and its blend, *International Journal of Corrosion and Scale Inhibition*, *8*(3), 744−759. https://doi.org/10.17675/2305-6894-2019-8-3-21

Thakur, A., Anadebe, V.C., Berdimurodov, E., Zarrouk, A., Dagdag, O., & Kumar, A. (2025). Understanding the chemistry and common issues of infrastructure corrosion, in Architectural Corrosion and Critical Infrastructure (eds. Aslam, R., Yan, Z, Wang, Q., & Aslam, J.), Royal Society of Chemistry, Chapter 1, pp. 1–34. https://doi.org/10.1039/9781837678259-00001

Thapa Kunwar Magar, K., Paudel, Y., Gautam, M., Bhattarai, N.P., & Bhattarai, J. (2025). Predictive assessment on the corrosion consequences of reinforced concrete frameworks available around Bhairahawa city areas (Nepal) with half-cell potential measurement. *Amrit Research*

Journal, *6*(1), 26–35. https://doi.org/10.3126/arj.v6i1.87528

Verma, C., Pathania, A.R., Barsoum, I., Rhee, K.Y., Qiang, Y., & Alfantazi, A. (2026). Coordination chemistry in corrosion science and engineering: role of coordination bonding and coordination materials. *Coordination Chemistry Review*s, *549*(1), 217258. https://doi.org/10.1016/j.ccr.2025.217258

Wilkie, S., & Dyer, T., 2021. Design and durability of early 20th century concrete bridges in Scotland: A review of historic test data. *International Journal of Architectural Heritage*, *16*(8), 1131–1151. https://doi.org/10.1080/15583058.2020.1870776

Zgura, I., Badea, N., Enculescu, M., Maraloiu, V.-A., Ungureanu, C., & Barbinta-Patrascu, M.-E. (2023). Burdock-derived composites based on biogenic gold, silver chloride and zinc oxide particles as green multifunctional platforms for biomedical applications and environmental protection. *Materials*, *16*, 1153. https://doi.org/10.3390/ma16031153

Zulkifli, F., Khairina, S., Ghazali, M.S.M., Al-Amiery, A.A., Ismail, N., Izionworu, V.O., Suriani, M.J., & Wan Nik, W.B. (2022). Application of electrochemical impedance spectroscopy technology to evaluate passivation performance of film forming and adsorption types corrosion inhibitors. *International Journal of Corrosion and Scale Inhibitor, 11*(3), 1303–1318. https://doi.org/10.17675/2305-6894-2022-11-3-23